Overview of State-of-the-Practice Modeling of Overconsolidated Soils

EMIR JOSE MACARI AND PEDRO ARDUINO

Numerical methods currently used in practice to predict the behavior of overconsolidated clays are described. The paper is not intended to be a state-of-the-art report but rather a state-of-the-practice report on techniques that have been used in practice. The discussion focuses on the Modified Cam Clay (MCC) model, which is widely accepted because of its practicality and simplicity. However, there are instances when more sophisticated overconsolidated soil models have been used. The paper presents an overview of the developments of soil elasto-plasticity followed by a detailed description of the MCC model and derivation of its incremental formulation. In addition, an example describing the calibration of the MCC parameters is presented. Step-by-step procedures are developed for drained and undrained predictions. A generalized form of the MCC model is described in which a third stress invariant is included in the formulation. A constitutive driver code is then implemented to allow for the numerical simulation of three-dimensional stress states. Finally, a brief description of the implementation of a constitutive driver into a finite element formulation is presented.

Traditionally, problems of soil mechanics have been divided into two groups: deformation problems and stability problems. The first group deals with the stress-strain, or load-deformation, of a soil mass before failure. Some of the problems that are considered in this category are stresses at a point in a soil mass under a structure, excavations, and settlement problems. Solutions to these problems have been obtained with the aid of the theory of linear elasticity because it has been assumed that small deformations produce a nearly linear elastic response of the soil mass. Stability problems, on the other hand, deal with the conditions of ultimate failure of a soil mass, and among these, one could list such problems as stability of slopes, earth pressure against lateral support, and bearing capacity of footings. The main issue related to stability problems is the determination of the loads that will cause failure of the structure or soil mass. In classical soil mechanics these problems have been solved by what is known as the theory of perfect plasticity or ultimate strength.

In the past few decades a third category of problems has emerged that is a combination of the first two problems, referred to as "progressive yielding." These problems deal with the theory of elasto-plasticity as soils deform from an initial elastic limit to an ultimate or critical state.

Initial attempts to model the mechanical behavior of soils have been attributed to Drucker et al. (*1*). This approach described the behavior of soil with constitutive equations using the framework of continuum mechanics. Researchers at the University of Cambridge (*2–4*) continued these efforts during the 1960s, leading to the framework of critical state soil mechanics (CSSM). Constitutive models such as the Cam Clay model (*3*) and the Modified Cam Clay (MCC) model (*5*) were developed on the basis of plasticity theory within the framework of CSSM. These models have been widely used because of their simplicity; however, there are many aspects of soil behavior that they fail to capture.

Over the last 20 years a great deal of effort has been dedicated to the development of more realistic constitutive models for soils. This emphasis is evident by the number of specialty conferences and prediction workshops that have been dedicated to modeling issues. There is a great deal of knowledge in the area of constitutive modeling of soils. However, as the models have become more and more advanced, so has the level of complexity increased. As a result these developments have had very limited impact on the practicing geotechnical engineering profession. In recent years these trends have reversed and there have been some efforts to incorporate the knowledge on constitutive modeling of soils into the actual practice of geotechnical engineering. Therefore emphasis has been placed on simplicity. The relationships between strain and stress (constitutive relations) have been implemented into finite element programs to solve engineering problems formulated as boundary-value problems.

Duncan (*6*) presented a summary of 100 publications in which advanced numerical models were used in practice for the analysis of the response of geotechnical structures. The models discussed in Duncan's paper ranged in complexity from very simple hyperbolic model formulations to more advanced models such as the MCC model and finally to more sophisticated models that incorporate failure theory into the analysis (shear band or bifurcation analysis). In addition, powerful pre- and postprocessors are being developed to aid the practicing engineer in gaining a better understanding of the response of earth structures as they are subjected to external loads or deformations within the context of finite element analysis. With these issues in mind, an attempt is made to demonstrate the need for advanced numerical models when dealing with overconsolidated soils. The main intent is to present some commonly used analytical methods and to explain how numerical (elastoplastic) soil models, specifically the MCC model, are implemented into displacement-based finite element techniques that may be used for the analysis of the response of earth structures. In so doing, an attempt is made to close the gap between research-driven developments in computational geomechanics and practical engineering.

SOIL MODELING

Although the number of soil models is too large to be described in detail here, the basic theories on which they are founded may be listed as follows (*7*):

School of Civil & Environmental Engineering, Georgia Institute of Technology, Atlanta, Ga. 30332-0355.

- Elasticity,
- Hyperbolic,
- Rate-type,
- Plasticity (single/multiyield surface),
- Plasticity (bounding surface), and
- Endochronic.

The formal mathematical theory of plasticity, originally presented by Hill (*8*), Prager and Hodge (*9*), Drucker (*10*), and others was developed to describe the mechanical response of metals. This theory has a tangible physical meaning for metals. However, as the theory was adapted to soils, which are pressure-sensitive materials because of the presence of voids, yielding was related to both mean effective stress as well as shear stresses, always including the effects of volume change.

However, even though there is no true physical definition for the theory of plasticity for soils, there is plenty of evidence to suggest that a reasonably good representation of the response of soils is obtained for normally consolidated clays (*11*). Hence, plasticity has become a widely used theory for modeling soil behavior. One of the most widely used plasticity models has been the MCC model (*5,12*). This model was originally developed for normally consolidated clays; however, it has also been used for overconsolidated clays. The response of highly overconsolidated soils predicted by MCC is governed by elastic behavior in the prepeak regime followed by a slight elastoplastic softening branch until the critical state is attained. This is a major shortcoming of this model. However, as stated earlier, the MCC model is one that is well understood and easily implemented.

DESCRIPTION OF MCC MODEL

Some important parameters used in the development of the Cam-Clay and MCC models are p', the mean effective stress; q, the stress difference (related to the octahedral shear stress or the second invariant of the deviatoric stress tensor); and e, the void ratio, or $v = 1 + e$, the specific volume. In a triaxial stress space one may express p' and q as $p' = (\sigma_1' + 2\sigma_3')/3$, $q = \sigma_1' - \sigma_3'$.

In an attempt to study the yielding behavior of normally consolidated clays, Roscoe et al. conducted tests on samples of saturated clays. The effective stress paths for several undrained tests were geometrically similar, and their ultimate stress states were observed to be on a straight line in a $q - p'$ space.

When a saturated soil sample is sheared, it experiences progressive states of yielding before reaching a state of collapse. That is, the stress path passes through several yield surfaces (hardening caps), causing plastic deformations. The yielding continues to occur until the material reaches a critical void ratio, after which it remains constant during subsequent deformations. That is, the material will pass through a state in which the arrangement of the particles is such that no volume change takes place during shearing. This particular void ratio is called the *critical void ratio* and is considered the ultimate state of the material. It has been observed that a soil with a void ratio lower than the critical value will deform in such a manner as to increase its volume, whereas at a void ratio higher than the critical value, the deformations will decrease in volume.

The MCC model is founded on the incremental plasticity theory, which provides stress-strain relationships that can be obtained by defining the four essential components of an elastic-plastic model: (*a*) Elastic properties; (*b*) yield surface (criterion); (*c*) plastic potential; (*d*) hardening rule.

Unloading and reloading of a soil is assumed to be elastic. That is, there is a linear relation between the specific volume (or void ratio) and the logarithm of the effective mean stress p', such that

$$\delta\epsilon_p^e = \kappa \frac{\delta p'}{v p'} \tag{1}$$

where κ is a model parameter similar to the swelling index and v is the specific volume $(e + 1)$.

Also, it assumed that the elastic shear strains result from any change in the deviator stress q such that

$$\delta\epsilon_q^e = \frac{\delta q}{3G} \tag{2}$$

where G is a constant shear modulus.

The yield criterion defines the limit of purely elastic behavior. When the state of stress comes in contact with the current yield surface, the material undergoes elastic-plastic deformations.

The MCC model yield surface is represented by an ellipse (Figure 1) given by

$$\frac{p'}{p_o'} = \frac{M^2}{M^2 + \eta^2} \tag{3}$$

where $\eta = q/p'$, p_o' is the isotropic preconsolidation stress, and M is the slope of the critical state line (failure envelope). As the soil yields p_o' increases (expanding the yield surface) and this increase is linked with changes in the effective stresses p' and q through the differential form of the yield function. The yield function can also be rewritten as

$$f = q^2 - M^2[p'(p_o' - p')] = 0 \tag{4}$$

The MCC model assumes that the soil obeys the normality condition (which essentially describes the ratio of shear to volumetric plastic strain increment as the soil yields). Therefore, the flow rule is associative and mathematically is simply given by the slope of a normal to the yield surface at the present stress state (shown in Figure 1) as

$$\frac{\delta\epsilon_p^p}{\delta\epsilon_q^p} = \frac{\partial g/\partial p'}{\partial g/\partial q} = \frac{M^2(2p' - p_o')}{2q} = \frac{M^2 - \eta^2}{2\eta} \tag{5}$$

as plastic deformations occur.

As the soil yields, it hardens, and this hardening is linked to the increase of the isotropic preconsolidation stress p_o'. This hardening relationship is assumed to be linear such that

$$v = N - \lambda \ln p_o' \tag{6}$$

where N is a model parameter that indicates the location of the isotropic compression in the $p' - v$ space (N is the value of v for the value of $\ln(p') = 0$ or $p' = 1$). Therefore, the magnitude of the plastic volumetric strains is given as

$$\delta\epsilon_p^p = [(\lambda - \kappa)/v] \frac{\delta p_o'}{p_o'} \tag{7}$$

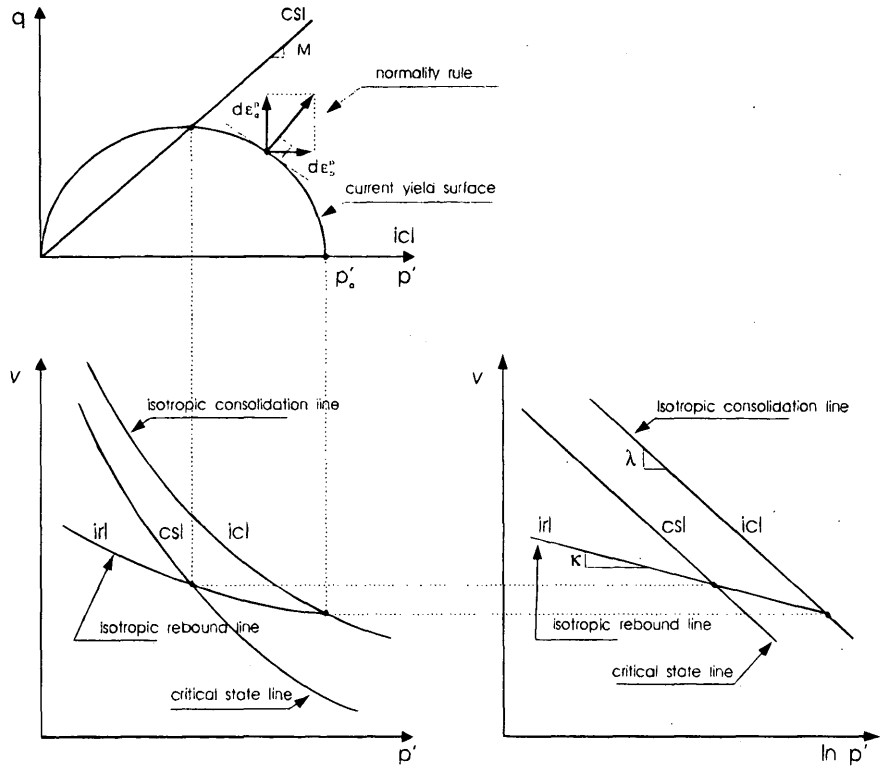

FIGURE 1 MCC yield and ultimate surfaces $p' - q$ and $p' - v$ spaces.

CALIBRATION OF MCC MODEL PARAMETERS AND PREDICTION

The calibration of the appropriate model parameters requires at least three undrained conventional triaxial compression (CTC) tests and one isotropic consolidation (IC) test. In addition, if one is interested in simulating the response of the soils in extension, one must also perform three undrained conventional triaxial compression (CTE) tests. As a way to illustrate the procedure, a testing program was designed to test a Speswhite clay under the above-mentioned conditions. The CTC and CTE tests were performed at confining pressures ranging from 50 to 800 kPa. Figure 2 presents the results of an isotropic consolidation test and superimposed are the values of λ, κ, and N. The results of the triaxial test program are presented in Figure 3, along with the predictions obtained from the MCC model. Figure 4 presents the test results in a $q - p'$ space for the 10 undrained shear tests. Note that the values of M_c and M_e can be readily obtained from the test data. Figure 4 also shows the response of the MCC model for each of the 10 test conditions.

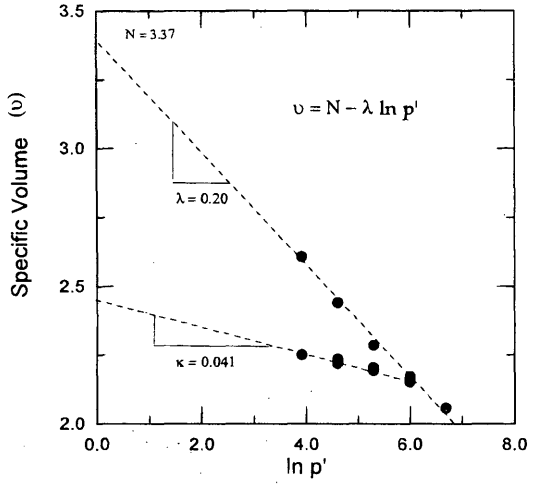

FIGURE 2 Results of isotropic consolidation test.

COMPUTATIONAL SEQUENCE FOR MCC MODEL

Drained Triaxial Test on Lightly Overconsolidated Clay

Given: The critical state parameters and the initial conditions: M, e_o, p'_o, p', G, K', κ, and λ; step-by-step procedure (Figure 5) is as follows:

1. Compute or note e_o on the Normally Consolidated Line (NC-Line) corresponding to p'_o.
2. Compute or note p'_X, e_X, and q_x for point X; the current Critical State Line (CSL)-Yield Surface intersection point.
3. Compute or note e_D for initial point D of test.
4. Compute e_U, q_U, and p'_U for the ultimate point U of the test.
5. Compute q_F and p'_F for the yield point F on the current yield locus.
6. Compute elastic strain components for path DF:

$$\Delta\epsilon_q^e = \frac{\Delta q}{3G} \qquad \Delta\epsilon_p^e = \frac{\kappa}{1 + e_o}\frac{\Delta p'}{p'} = \kappa'\frac{\Delta p'}{p'}$$

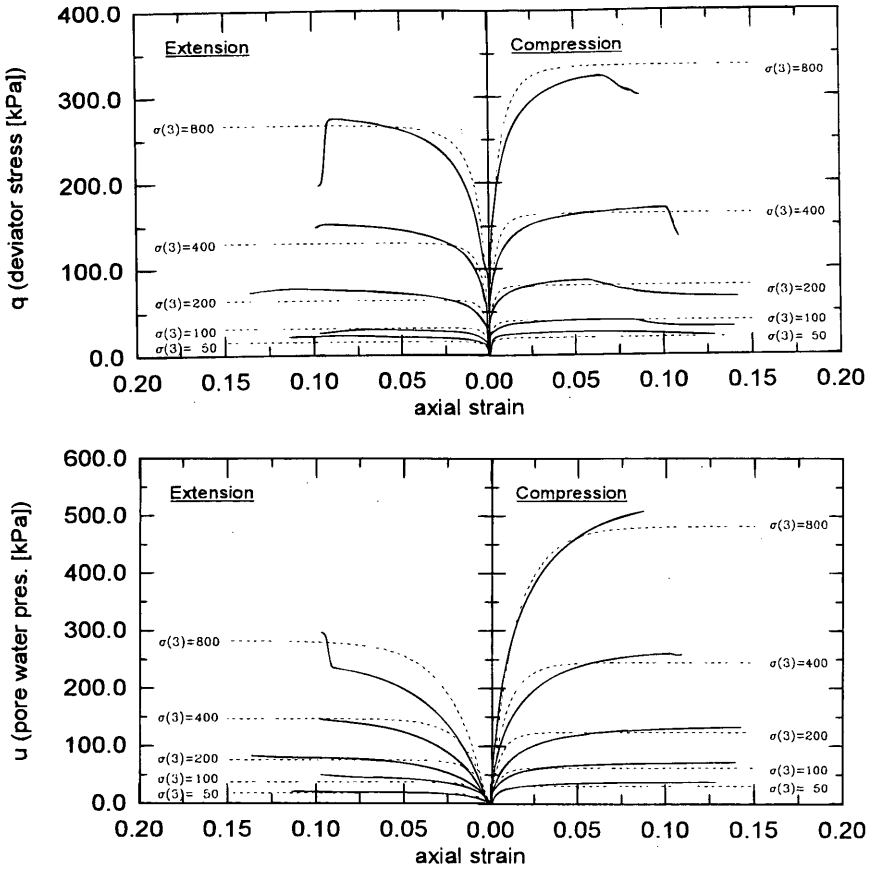

FIGURE 3 Stress-strain (*top*) and pore-water pressure (*bottom*) results of CTC and CTE tests and MCC model predictions.

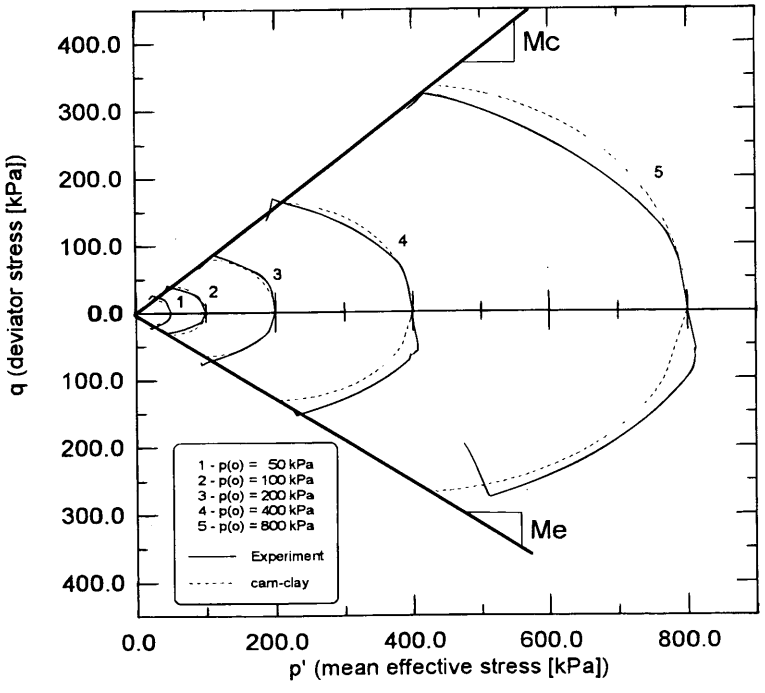

FIGURE 4 Results of CTC and CTE tests and MCC model predictions in $q - p'$ space.

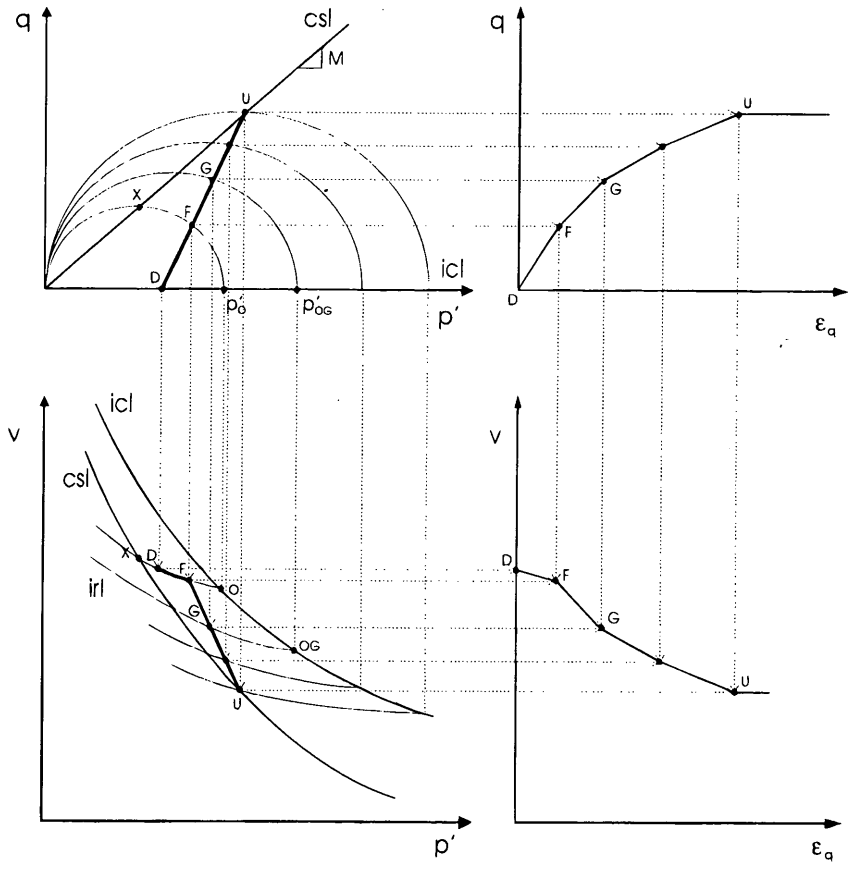

FIGURE 5 Stress paths for MCC model prediction of drained triaxial test on lightly overconsolidated clay.

7. Select several equal stress increments (three or more) along the stress path between F and U.
8. Compute coordinates p'_G and q_G of intermediate point G.
9. Compute coordinates p'_{OG} corresponding to new yield locus through G:

$$p'_{OG} = p'_G\left[\left(\frac{qG}{Mp'_G}\right)^2 + 1\right]$$

which comes from $M^2 p'_{OG} p'_G = p'^2_G M^2 + q^2_G$.

10. Find e_{OG} corresponding to p'_{OG} on the NC-Line.
11. Find e_G on the recompression line through OG.
12. Compute

$$\Delta\epsilon_p^{\text{total}} = \frac{\Delta e}{1 + e_o}$$

13. Compute

$$\Delta\epsilon_p^e = \kappa' \frac{\Delta p'}{p'}$$

14. Compute

$$\Delta\epsilon_p^p = \Delta\epsilon_p - \Delta\epsilon_p^e$$

15. Compute plastic shear strain increment $\Delta\epsilon_q^p$ from the Normality Law:

$$\Delta\epsilon_q^p = \Delta\epsilon_p^p\left[\frac{qG}{M^2\left(p'_G - \frac{p'_{OG}}{2}\right)}\right]$$

16. Compute elastic shear strain increment as in Step 6:

$$\Delta\epsilon_q^e = \frac{\Delta q}{3G}$$

17. Then $\Delta\epsilon_q^{\text{total}} = \Delta\epsilon_q^e + \Delta\epsilon_q^p$.
18. Repeat Steps 8–15 for point H and any subsequent or intermediate points before U is reached.
19. Plot q versus $\Delta\epsilon_q^{\text{total}}$ and e versus $\epsilon_q^{\text{total}}$.

Undrained Triaxial Test on Lightly Overconsolidated Clay

Given: The critical state parameters and the initial conditions: M, e_o, p'_o, p', G, K', κ, and λ; step-by-step procedure (Figure 6) is as follows:

1. Compute or note initial yield surface from p'_o.

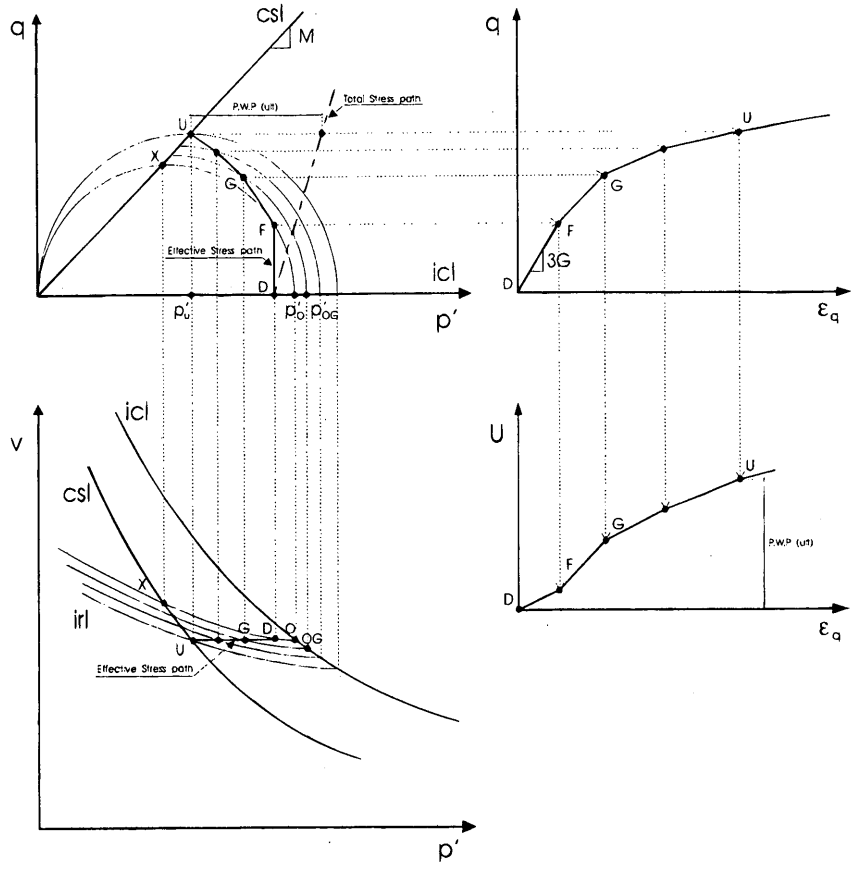

FIGURE 6 Stress paths for MCC model prediction of undrained triaxial test on lightly overconsolidated clay.

2. Compute e_o for initial point D of the test.
3. Compute or note p'_U corresponding to $e_D = e_D$ on CSL; also note q_U.
4. Compute q_F, and p'_F for the yield point F on the current yield locus. Since the behavior is purely elastic and $\Delta V = \Delta\epsilon_p = 0$, the $\Delta p' = 0$ and DF is vertical.
5. Compute

$$\Delta\epsilon_q^e = \frac{\Delta q}{3G} \qquad \Delta u = \Delta p \; (\Delta p' = 0)$$

6. Construct the new yield surface through a selected intermediate point G.
7. From

$$p'_{OG} = p'_G \left[\left(\frac{qG}{Mp'_G} \right)^2 + 1 \right]$$

find the new OG at the intersection of the recompression line through G and the NC-Line. Construct new yield locus. Compute qG corresponding to G.
8. Compute

$$\epsilon_p^p = -\epsilon_p^e = -\kappa' \frac{\Delta'_p}{p'}, \text{ since } \Delta\epsilon_p = 0$$

9. Use the Normality Law to compute $\Delta\epsilon_q^p$:

$$\Delta\epsilon_q^p = \Delta\epsilon_p^p \left[\frac{qG}{M^2 \left(p'_G - \frac{p'_{OG}}{2} \right)} \right]$$

10. Use: $\Delta\epsilon_q^{\text{total}} = \Delta\epsilon_q^e + \Delta\epsilon_q^p$.
11. Compute the increment of the pore pressure as $\Delta u = \Delta p - \Delta p'$.
12. Repeat Steps 7–11 for additional increments.
13. Plot q versus $\epsilon_q^{\text{total}}$ and u versus $\epsilon_q^{\text{total}}$.

IMPLEMENTATION OF THIRD STRESS INVARIANT

To properly account for the three-dimensionality of the stress space, one should include a third stress invariant in the formulation in addition to the two (p' and q) mentioned previously. This third invariant will account for the nonsymmetric shape of the observed yield function in the principal (or octahedral) stress space. One convenient form of the third stress invariant proposed is the so-called lode angle (θ), which gives the angle between the principal stress direction and the current stress path. If one maintains that $\sigma_1 \geq \sigma_2 \geq \sigma_3$, it will suffice to describe the lode angle θ from 0 to 60 degrees, which can be expressed as

$$\cos(3\theta) = \frac{9}{2}\frac{\mathrm{tr}(\sigma_d^3)}{q^3}$$

The MCC model yield function (Equation 4) takes the form

$$f = q^2 g^2(\theta) + M^2 p'^2 - M^2 p' p'_o = 0 \tag{8a}$$

where $g(\theta)$ is a function that defines the shape of the yield function in the deviatoric plane and was originally proposed by Willam and Warnke (*13*):

$$g(\theta) = \frac{4(1-e^2)\cos^2\left(\frac{\pi}{3}-\theta\right)+(2e-1)^2}{2(1-e^2)\cos\left(\frac{\pi}{3}-\theta\right)+(2e-1)\left[4(1-e^2)\cos^2\left(\frac{\pi}{3}-\theta\right)+5e^2-4e\right]^{1/2}} \tag{8b}$$

The eccentricity parameter e must satisfy the condition $1/2 \leq e \leq 1$ in order to maintain a convex yield surface. One may define e as the ratio of the shear strength in extension to that in compression. For $e = 1$, i.e., $g(\theta) = 1$, the influence of the third stress invariant via θ is dropped and the now-conical surface becomes a circle in the deviatoric plane. As the value of e approaches $1/2$, the shape of the yield surface becomes more triangular (*14*).

Within the context of the finite element method, it is often convenient to utilize implicit integration techniques (as opposed to the above-mentioned explicit integration) for the solution of unknown stress paths that might develop in a boundary value problem. Implicit integration techniques do not restrict the size of the integration step resulting in a more robust algorithm that can account for larger deformations as compared with the explicit integration techniques (*14*). One implicit integration technique that has gained wide acceptance is that referred to as the Closest-Point-Projection Method (CPPM). For a detailed presentation of this technique, the reader is referred to work by Alawaji et al. (*14*).

The CPPM algorithm was implemented in a mixed-control (stress- and strain-controlled) driver computer code in conjunction with a generalized three-stress invariant MCC model (described previously). Several examples of triaxial stress paths were selected to illustrate the simulation of CTC and CTE tests on normally and overconsolidated clay specimens, as shown in Figures 7–9. The simulations performed represent undrained test conditions. The undrained condition is obtained by subjecting the analysis to an incompressibility constraint in addition to the imposed stress equilibrium conditions.

Figures 9 and 10 present the results of a simulation of specimens tested under CTC conditions under identical confining stress level (20 kPa). Figure 10 shows the results in a $q - p'$ space and presents how the MCC model simulates the overconsolidation of soil specimens. That is, for the normally consolidated state the specimen undergoes plastic strain from the onset of shearing; however, the overconsolidated specimens undergo initial elastic deformation until they reach a stress state compatible with their original yield surface (governed by their preconsolidation stress). It is interesting to note that the specimen having an overconsolidation ratio of 2 undergoes only elastic deformation until it reaches the critical state and then undergoes continuous plastic flow. Figure 10 presents the same results as deviator stress-axial strain and pore-water pressure-axial strain.

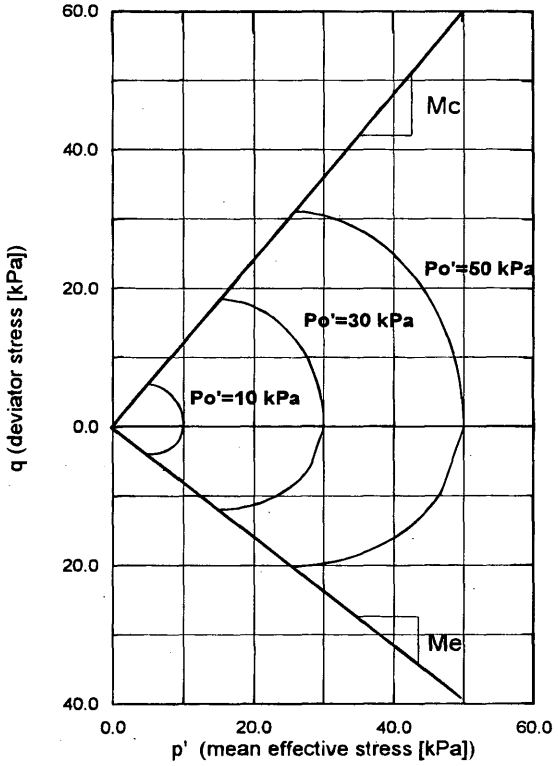

FIGURE 7 Simulation of CTC and CTE tests on normally consolidated clay specimens.

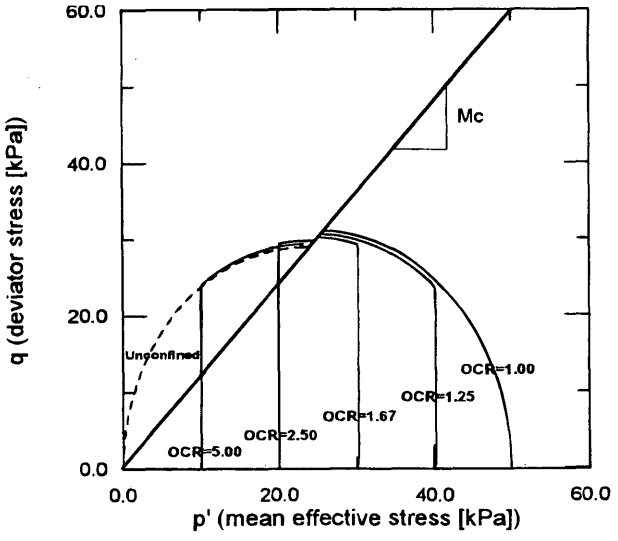

FIGURE 8 Simulation of CTC tests on overconsolidated clay specimens.

FINITE ELEMENT IMPLEMENTATION

In many geotechnical problems it is important to determine the distribution of stresses and displacements throughout the soil structure. In the determination of a system of stresses and displacements for a given problem, one must first define the corresponding governing equations that should satisfy the conditions of equilibrium and com-

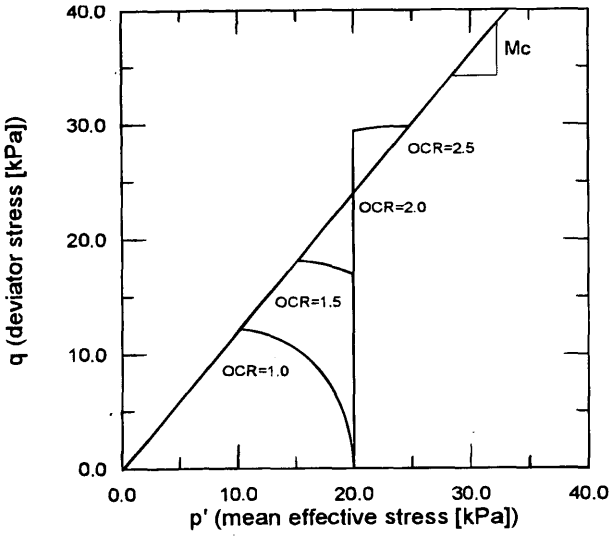

FIGURE 9 Simulation of CTC tests on normally and overconsolidated clay specimens subjected to confining levels of 20 kPa.

patibility. A basic difficulty in this regard, quite different from the solvability of the governing equations, is their ability to represent in situ conditions. Complications in geometry, loading, and material properties contribute to the problem.

The exact solution of the resulting equations, which in general are partial differential equations that satisfy all boundary conditions, is only possible for relatively simple systems, and numerical procedures are commonly employed to predict the system response.

The most common numerical procedure used to address these problems is the finite element method. This consists of the subdivision of the continuum into regions (finite elements) for which the behavior is described by a separate set of assumed functions representing stresses or displacements (*15,16*). These sets of functions are often chosen in a form that ensures continuity of the described behavior throughout the complete continuum. Certain types of finite element algorithms require no knowledge of the material model being used, or the constitutive strategy at the constitutive level. The constitutive formulation must only update stresses and state variables to the finite element level, given the current stresses, state variables, and strain increment. This makes the incorporation of additional constitutive models into the finite element formulation easy.

CONCLUSIONS

This paper has focused on the MCC model, because it is one that has been widely accepted in practice due to its simplicity and "real" physical representation. A generalized form of the MCC model was described where a third stress invariant was included in the formulation. A brief parametric study was presented to show how the MCC model may simulate the response of normally, lightly and highly overconsolidated clays. However, as previously mentioned, there are instances when more sophisticated models may be warranted, especially for highly overconsolidated soil models. From the examples presented in this paper it is evident that the MCC model cannot properly account for the essential characteristics of highly overconsolidated clays. Some of the limitations of the MCC model are as follows.

- During undrained loading shearing of overconsolidated clays, the MCC model predicts linear elastic response for stress states within the current yield surface. In the case of highly overconsolidated clays this linear elastic response is up to peak. The yield point is marked by a sharp change in the tangential stiffness, and the critical state is tangentially approached.
- The MCC model describes uncoupled behavior which result in no shear-induced pore pressure response predictions during

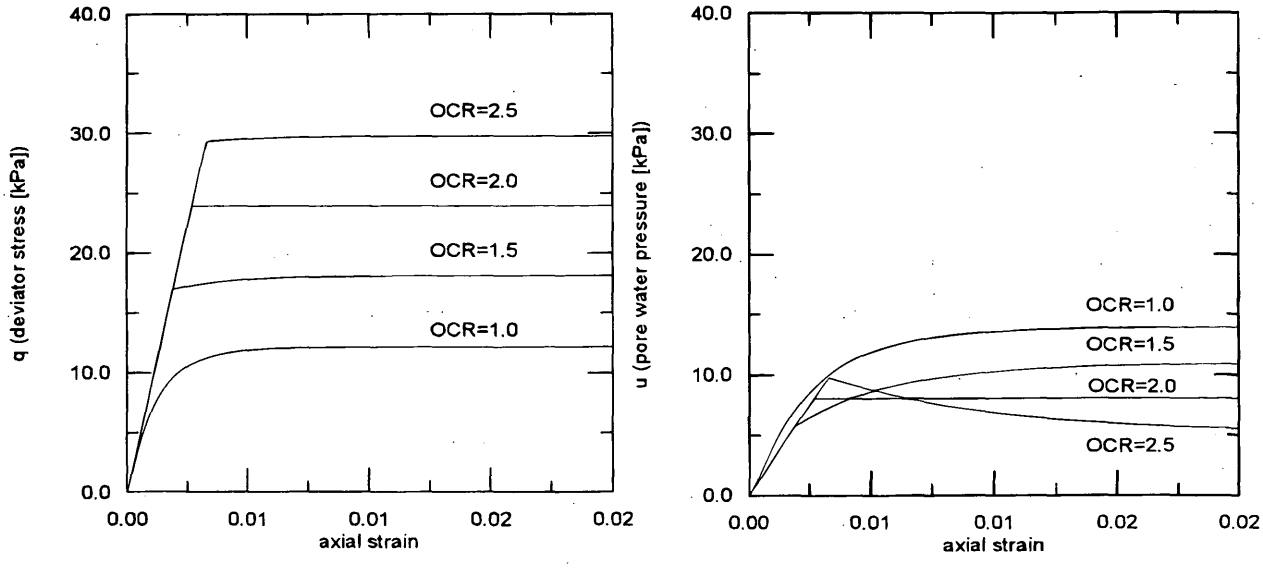

FIGURE 10 Stress-strain-pore-water pressure response of normally and overconsolidated clay specimens subjected to confining levels of 20 kPa.

undrained loading. Therefore it is very difficult for the MCC model to predict the negative pore pressures that highly overconsolidated clays may exhibit during undrained shear.

In recent years there have been some innovative models developed that are capable of simulating the dilatant tendency of overconsolidated clays. However, the complexities in these newer formulations have also made them less desirable to the practicing engineer and will continue to do so until constitutive modelers return to the ideology that simplicity is better. A good compromise between sophistication and simplicity will result in the closure of the gap that today exists between the state-of-the-art and the state-of-the-practice in constitutive modeling of soils. In recent years, researchers have attempted to develop a unified approach to constitutive modeling (i.e., the development of models that may be suitable for different soil types under a variety of stress states and history). This shift in philosophy will surely improve the chances that engineers may again view developments in constitutive modeling as something they should consider for the analysis of practical problems and not as yet another constitutive model.

REFERENCES

1. Drucker, D. C., R. Gibson, and D. J. Henkel. Soil Mechanics and Work Hardening Theories of Plasticity. *Transactions of the American Society of Civil Engineers,* Vol. 122, 1957, pp. 338–346.
2. Roscoe, K. H., A. N. Schofield, and C. P. Wroth. On the Yielding of Soils. *Geotechnique*, Vol. 8, 1958, pp. 22–53.
3. Roscoe, K. H., A. N. Schofield, and A. Thurarajah. Yielding of Clays in States Wetter than Critical. *Geotechnique*, Vol. 13, No. 3, 1963, pp. 211–214.
4. Schofield, A. N., and C. P. Wroth. *Critical State Soil Mechanics.* McGraw Hill, London, 1968.
5. Roscoe, K. H., and J. B. Burland. On the Generalized Stress-Strain Behavior of Wet Clays. In *Engineering Plasticity* (J. Heyman and F. A. Leckie, eds.), Cambridge University Press, Cambridge, UK, 1968, pp. 535–609.
6. Duncan, J. M., The Role of Advanced Constitutive Relations in Practical Applications. *Proceedings of the XIII International Conference ICSMFE*, New Delhi, India, Vol. 5, Jan. 1994, pp. 31–48.
7. Bardet, J. P. *Application of Plasticity Theory to Soil Behavior: A New Sand Model.* Ph. D. dissertation. California Institute of Technology, Pasadena, 1983.
8. Hill, R. *The Mathematical Theory of Plasticity.* Clarendon Press, Oxford, 1950.
9. Prager, W., and P. G. Hodge. *Theory of Perfectly Plastic Solids.* Dover, New York, 1951.
10. Drucker, D. C. A More Fundamental Approach to Plastic Stress-Strain Relations. *Proceedings of the 1st U. S. National Congress of Applied Mechanics*, ASME, Vol. 1, 1951, pp. 487–491.
11. Lewin, P. I., and J. B. Burland. Stress-Probe Experiments on Saturated Normally Consolidated Clay. *Geotechnique*, Vol. 20, No. 1, 1970, pp. 38–56.
12. Wood, D. M. *Soil Behaviour and Critical State Soil Mechanics.* Cambridge University Press, Cambridge, UK, 1990.
13. Willam, K. J., and E. P. Warnke. Constitutive Model for Triaxial Behavior of Concrete. *Colloquium on Concrete Structures Subjected to Triaxial Stresses*, ISMES, Bergamo, IABSE Report Vol. 19, 1974.
14. Alawaji, H., K. Runesson, and S. Sture. Integration of Constitutive Equations in Soil Plasticity. *Journal of Engineering Mechanics*, ASCE, Vol. 117, No. 8, 1991, pp. 1771–1790.
15. Zienkiewicz, O. C., and R. L. Taylor. *The Finite Element Method*, 4th Edition, Vol. 1 and Vol. 2, McGraw Hill, United Kingdom, 1991.
16. Bathe, K. J. *Finite Element Procedures in Engineering Analysis.* Prentice-Hall, Inc., Englewood Cliffs, N.J., 1981.

APPENDIX

Incremental Relations for MCC Model

During the process of yielding, the material hardens and the yield surface expands to a new position. In order to describe the elasto-plastic response of the soil, it is essential that one develop explicit relations in an incremental (flow) fashion. These formulations will then be used to predict the response of a soil as the stresses or strains are incrementally increased or decreased. Hence, the objective is to develop explicit incremental stress-strain relations of the form

$$\tilde{\boldsymbol{\sigma}} = \boldsymbol{C}^{ep}\,\tilde{\boldsymbol{\epsilon}} \tag{A1a}$$

or

$$\begin{Bmatrix} dq \\ dp' \end{Bmatrix} = \begin{bmatrix} C \end{bmatrix}^{ep} \begin{Bmatrix} d\epsilon_q \\ d\epsilon_p \end{Bmatrix} = \left(\begin{bmatrix} C \end{bmatrix}^{e} - \begin{bmatrix} C \end{bmatrix}^{p} \right) \begin{Bmatrix} d\epsilon_q \\ d\epsilon_p \end{Bmatrix} = \begin{bmatrix} C_{11} & C_{12} \\ C_{21} & C_{22} \end{bmatrix} \begin{Bmatrix} d\epsilon_q \\ d\epsilon_p \end{Bmatrix} \tag{A1b}$$

From the additive strain decomposition:

$$\epsilon_q = \epsilon_q^e + \epsilon_q^p \qquad d\epsilon_q = d\epsilon_q^e + d\epsilon_q^p \tag{A2}$$

$$\epsilon_p = \epsilon_p^e + \epsilon_p^p \qquad d\epsilon_p = d\epsilon_p^e + d\epsilon_p^p \tag{A3}$$

Hooke's law for isotropic and linear elastic materials gives

$$dq = 3Gd\epsilon_q^e \qquad dp' = K'd\epsilon_p^e \tag{A4}$$

$$\tilde{\boldsymbol{\sigma}} = \boldsymbol{C}^{e}\,\tilde{\boldsymbol{\epsilon}}^{e} \tag{A5}$$

or

$$\begin{Bmatrix} dq \\ dp' \end{Bmatrix} = \begin{bmatrix} 3G & 0 \\ 0 & K' \end{bmatrix} \begin{Bmatrix} d\epsilon_q^e \\ d\epsilon_p^e \end{Bmatrix} \tag{A6}$$

Flow Rule: Associated Flow (the plastic potential is the same as the yield surface $f = g$)

$$d\epsilon_q^p = d\Lambda \frac{\partial f}{\partial q} \tag{A7a}$$

$$d\epsilon_p^p = d\Lambda \frac{\partial f}{\partial p'} \tag{A7b}$$

Yield Function and Consistency Condition:

$$f = f(\sigma_{ij}, \kappa) \leq 0 \tag{A8a}$$

Here

$$df = \frac{\partial f}{\partial q} dq + \frac{\partial f}{\partial p'} dp' + \frac{\partial f}{\partial p_o'} dp_o' = 0 \tag{A8b}$$

$$f = f(q, p', p_o') \leq 0 \tag{A8c}$$

Hardening Rule:

$$d\epsilon_p^p = d\epsilon_p - d\epsilon_p^e = \frac{\lambda dp_o'}{p_o'(1 + e_o)} - \frac{\kappa dp_o'}{p_o'(1 + e_o)} \tag{A9a}$$

or

$$d\epsilon_p^p = \frac{(\lambda - \kappa)dp_o'}{p_o'(1 + e_o)} \tag{A9b}$$

$$dp_o' = \frac{p_o'(1 + e_o)}{(\lambda - \kappa)}\, d\epsilon_p^p \tag{A9c}$$

From Equations A3, A4, and A6 we obtain

$$\begin{Bmatrix} dq \\ dp' \end{Bmatrix} = \begin{bmatrix} 3G & 0 \\ 0 & K' \end{bmatrix} \left(\begin{Bmatrix} d\epsilon_q \\ d\epsilon_p \end{Bmatrix} - \begin{Bmatrix} d\epsilon_q^p \\ d\epsilon_p^p \end{Bmatrix} \right) \tag{A10a}$$

or

$$dq = 3G(d\epsilon_q - d\epsilon_q^p) \tag{A10b}$$

and

$$dp' = K'(d\epsilon_q - d\epsilon_p^p) \tag{A10c}$$

From Equations A7a and A7b

$$dq = 3G\left(d\epsilon_q - d\Lambda \frac{\partial f}{\partial q}\right) \qquad dp' = K'\left(d\epsilon_p - d\Lambda \frac{\partial f}{\partial p'}\right) \tag{A11}$$

Substituting Equation A11 and Equation A9c into Equation 14b one obtains

$$\frac{\partial f}{\partial q} 3G\left(d\epsilon_q - d\Lambda \frac{\partial f}{\partial q}\right) + \frac{\partial f}{\partial p'} K'\left(d\epsilon_p - d\Lambda \frac{\partial f}{\partial p'}\right) + \frac{\partial f}{\partial p_o'} \frac{p_o'(1 + e_o)}{(\lambda - \kappa)}\, d\Lambda \frac{\partial f}{\partial p'} = 0 \tag{A12}$$

Rearranging Equation A12 and solving for $d\Lambda$ results in

$$d\Lambda = \frac{\frac{\partial f}{\partial q} 3G d\epsilon_q + \frac{\partial f}{\partial p'} K' d\epsilon_p}{\frac{\partial f}{\partial q} 3G \frac{\partial f}{\partial q} + \frac{\partial f}{\partial p'} K' \frac{\partial f}{\partial p'} - \frac{\partial f}{\partial p_o'} \frac{p_o'(1 + e_o)}{(\lambda - \kappa)} \frac{\partial f}{\partial p'}} \tag{A13a}$$

or

$$d\Lambda = \frac{\begin{bmatrix} \frac{\partial f}{\partial q}, \frac{\partial f}{\partial p'} \end{bmatrix} \begin{bmatrix} 3G & 0 \\ 0 & K' \end{bmatrix} \begin{Bmatrix} d\epsilon_q \\ d\epsilon_p \end{Bmatrix}}{\begin{bmatrix} \frac{\partial f}{\partial q'} & \frac{\partial f}{\partial p'} \end{bmatrix} \begin{bmatrix} 3G & 0 \\ 0 & K' \end{bmatrix} \begin{Bmatrix} \frac{\partial f}{\partial q} \\ \frac{\partial f}{\partial p'} \end{Bmatrix} - \frac{\partial f}{\partial p_o'} \frac{p_o'(1 + e_o)}{(\lambda - \kappa)} \frac{\partial f}{\partial p'}} \tag{A13b}$$

This expression can then be substituted into Equations A6 and A11 to obtain

$$\tilde{\boldsymbol{\sigma}} = [\mathbf{C}^e - \mathbf{C}^p]\, \tilde{\boldsymbol{\epsilon}} \tag{A14a}$$

$$\begin{Bmatrix} dp \\ dp' \end{Bmatrix} = \left(\begin{bmatrix} C^e \end{bmatrix} - \begin{bmatrix} C^p \end{bmatrix} \right) \begin{Bmatrix} d\epsilon_q \\ d\epsilon_p \end{Bmatrix} \tag{A14b}$$

where

$$\begin{bmatrix} C^e \end{bmatrix} = \begin{bmatrix} 3G & 0 \\ 0 & K' \end{bmatrix} \tag{A14c}$$

and

$$\begin{bmatrix} C^p \end{bmatrix} = \frac{\begin{bmatrix} 3G & 0 \\ 0 & K' \end{bmatrix} \begin{Bmatrix} \frac{\partial f}{\partial q} \\ \frac{\partial f}{\partial p'} \end{Bmatrix} \begin{bmatrix} \frac{\partial f}{\partial q'} & \frac{\partial f}{\partial p'} \end{bmatrix} \begin{bmatrix} 3G & 0 \\ 0 & K' \end{bmatrix}}{\begin{bmatrix} \frac{\partial f}{\partial q'} & \frac{\partial f}{\partial p'} \end{bmatrix} \begin{bmatrix} 3G & 0 \\ 0 & K' \end{bmatrix} \begin{Bmatrix} \frac{\partial f}{\partial q} \\ \frac{\partial f}{\partial p'} \end{Bmatrix} - \frac{\partial f}{\partial p_o'} \frac{p_o(1 + e_o)}{(\lambda - \kappa)} \frac{\partial f}{\partial p'}} \tag{A14d}$$

Knowing the yield function f from Equation 4 one can differentiate to obtain the appropriate ratios:

$$\frac{\partial f}{\partial q} = 2q, \qquad \frac{\partial f}{\partial p'} = 2M^2 p' - M^2 p_o', \qquad \frac{\partial f}{\partial p_o'} = -M^2 p' \tag{A15}$$

Substituting into Equation A14d results in

$$\begin{bmatrix} C^p \end{bmatrix} = \frac{\begin{bmatrix} 3G & 0 \\ 0 & K' \end{bmatrix} \begin{Bmatrix} 2q \\ 2M^2 p' - M^2 p_o' \end{Bmatrix} [2q,\ 2M^2 p' - M^2 p_o'] \begin{bmatrix} 3G & 0 \\ 0 & K' \end{bmatrix}}{[2q,\ 2M^2 p' - M^2 p_o'] \begin{bmatrix} 3G & 0 \\ 0 & K' \end{bmatrix} \begin{Bmatrix} 2q \\ 2M^2 p' - M^2 p_o' \end{Bmatrix} - \frac{-M^2 p' p_o'(1 + e_o)}{(\lambda - \kappa)} 2M^2 p' - M^2 p_o'} \tag{A16}$$

Finally, if one executes the matrix multiplication and expand its terms, one obtains

$$\begin{Bmatrix} dq \\ dp' \end{Bmatrix} = \left(\begin{bmatrix} 3G & 0 \\ 0 & K' \end{bmatrix} - \begin{bmatrix} C^p \end{bmatrix} \right) \begin{Bmatrix} d\epsilon_q \\ d\epsilon_p \end{Bmatrix} \tag{A17a}$$

where

$$\begin{bmatrix} C^p \end{bmatrix} = \frac{1}{h} \begin{bmatrix} 36G^2 q^2 & 6GK' M^2 q(2p' - p_o') \\ 6GK' M^2 q(2p' - p_o') & K'^2 M^4 (2p' - p_o')^2 \end{bmatrix} \tag{A17b}$$

and where

$$h = 12Gq^2 + K' M^4 (2p' - p_o')^2 + \frac{M^4 p' p_o'(1 + e_o)(2p' - p_o')}{(\lambda - \kappa)} \tag{A17c}$$

Equations A17a, A17b, and A17c represent the explicit integration formulation of the MCC model.